Journal of CO2 Utilization 105 (2026) 103335

Contents lists available at ScienceDirect

Journal of CO2 Utilization

journal homepage: www.elsevier.com/locate/jcou

Molecular dynamics study on the mechanisms of ultrafine bubbles in CO_2 hydrate formation

Hamidreza Hassanloo *, Xinyan Wang

Centre for Advanced Powertrain and Fuels, Brunel University of London, Uxbridge UB8 3PH, United Kingdom

ARTICLE INFO

Keywords:
Carbon capture
CO_2 hydrate
Nanobubbles
Growth mechanism
Molecular dynamics simulation

ABSTRACT

The accelerating rise in atmospheric CO_2, driven by anthropogenic emissions, necessitates urgent mitigation strategies. Among carbon capture and storage (CCS) technologies, CO_2 hydrate-based methods offer a promising pathway for efficient sequestration, storage, and utilization. However, the inherently slow kinetics of hydrate nucleation and growth limit their practical application. This study explores the use of various nanobubbles (NBs), including hydrogen, nitrogen, oxygen, and carbon dioxide, as stable, nanoscale gas cavities that act as novel promoters to enhance CO_2 hydrate formation, using molecular dynamics (MD) simulations. The results demonstrate that under optimal thermodynamic conditions, the presence of NBs significantly enhances hydrate formation. This enhancement is attributed to the hydrophobic NB surfaces acting as nucleation spots, promoting local concentration gradients and accelerating clathrate formation kinetics, while reducing the likelihood of random nucleation events in the bulk phase. Due to their smaller molecular sizes, hydrogen and nitrogen NBs further facilitate hydrate formation by diffusing into the solution from the NB core. However, lower temperature, as a primary sub-optimal thermal condition, reduce molecular mobility and suppress these mechanisms, thereby hindering hydrate growth. At elevated pressures, NBs exhibit a dual role, both promoting and inhibiting hydrate formation, and the comparison with non-nanobubbled samples reveals a pressure-dependent shift in the dominant nucleation mechanism from NB-induced interfacial ordering to bulk-phase interactions.

1. Introduction

The escalating atmospheric carbon dioxide (CO_2) concentration, predominantly driven by anthropogenic emissions, is a critical driver of global climate change, necessitating urgent and effective mitigation strategies [1]. The Intergovernmental Panel on Climate Change (IPCC) reports that climate change has already caused substantial disruptions in ecosystems and biodiversity. In response, the Paris Agreement has set an ambitious yet essential goal to limit global warming to well below 2 °C, with efforts to restrict it further to 1.5 °C in order to mitigate the adverse impacts of greenhouse gas (GHG) emissions [2]. Achieving carbon neutrality, as underscored in the IPCC Special Report on Global Warming of 1.5°C, necessitates the prompt peaking of global carbon emissions. In 2019, global CO_2 emissions reached an unprecedented 43.1 gigatonnes (Gt) [3]. Carbon capture and storage (CCS) technologies have emerged as essential components of climate mitigation strategies, offering not only significant reductions in greenhouse gas emissions but also broader economic and environmental benefits in the transition to net-zero energy systems [4]. However, the overall effectiveness and long-term sustainability of CCS remain subjects of active scientific discussion, particularly concerning its large-scale impacts on the carbon and oxygen cycles, as well as its energy and resource requirements [5].

Among all CCS technologies, CO_2 hydrate stands out as a novel approach that not only enables effective carbon capture but also offers valuable applications such as gas storage, transportation, and use as a secondary refrigerant, owing to its high dissociation enthalpy and environmentally friendly properties [6]. Clathrate hydrates are ice-like crystalline solid inclusion compounds formed when water molecules act as hosts, encapsulating guest gas species within a hydrogen-bonded lattice under specific pressure–temperature conditions. These structures consist of various cage topologies required to occupy three-dimensional space, with three primary hydrate families classified according to the size of the largest guest molecules. The stability of clathrate hydrates is primarily governed by short-range attractive interactions between the guest molecules, often paradoxically hydrophobic, and the surrounding water cages. Additionally, hydrogen bonding and other intermolecular interactions contribute to the structural and dynamic properties of the hydrates. In the context of CO_2 hydrates, the formation kinetics involve

* Corresponding author.
E-mail address: Hamidreza.Hassanloo@brunel.ac.uk (H. Hassanloo).

https://doi.org/10.1016/j.jcou.2026.103335
Received 22 August 2025; Received in revised form 15 October 2025; Accepted 18 January 2026
Available online 21 January 2026

nucleation followed by crystal growth. However, the inherently slow rates of hydrate nucleation and growth present significant challenges. While physical methods such as pressurization, cooling, and agitation have been employed to enhance formation, these approaches are typically energy-intensive, limited in scalability, and economically impractical. Consequently, the use of chemical additives has emerged as a promising and more efficient strategy to overcome these limitations and accelerate hydrate formation [7,8].

Nanobubbles (NBs) have recently gained attention as a promising alternative to conventional enhancement techniques, particularly in the formation of natural gas hydrates [9]. These nanoscale gas-filled cavities, typically less than 1 μm in diameter and often exhibiting a spherical cap morphology, can exist either as surface-adhered NBs or dispersed within bulk liquid solutions. They can be generated through various techniques, including cavitation, electrolysis, ethanol–water exchange, and membrane-based methods. The unique physicochemical properties of NBs, such as their exceptional stability, high surface-to-volume ratio, enhanced mass transfer efficiency, and capacity to generate free radicals, make them particularly well-suited for promoting hydrate nucleation via heterogeneous mechanisms [10–12]. These attributes position NBs as a valuable and energy-efficient tool for improving the kinetics of hydrate formation, offering significant potential for scaling up clathrate-based gas storage and separation technologies.

In recent years, increasing research attention has been directed toward the impact of additives on CO_2 hydrate formation kinetics, reflecting the multidisciplinary nature of gas hydrate studies that span from the molecular scale to reservoir-scale applications [8,13]. Experimental methods, including ultrasonic technology [14], Raman spectroscopy [15], and micromodels [16], have been widely employed to investigate hydrate formation and growth behavior. Notably, the influence of microscale bubbles on hydrate formation has been examined using a transparent acrylic water tank equipped with a CCD camera system, revealing that their high gas-dissolution capacity and size-dependent internal pressure facilitate real-time hydrate nucleation and growth under milder conditions [17]. These techniques provide valuable macroscopic insights but are often limited in their ability to directly capture the microscopic processes involved in hydrate nucleation and stabilization. As a result, optimization of parameters in hydrate-related engineering processes often proceeds, at least initially, through empirical trial-and-error approaches. However, the complexity of these systems eventually necessitates a fundamental understanding that reaches down to the molecular level [8]. Given the challenges associated with acquiring direct experimental evidence at this scale, hydrate nucleation has emerged as a prime subject for molecular-level investigation, particularly through molecular dynamics (MD) simulations. MD simulations serve as a powerful tool to explore the microscopic mechanisms of gas hydrate systems, providing insight into nucleation, growth, stability, interfacial characteristics, additive effects, and both thermodynamic and kinetic properties [13]. Previous MD studies have explored various additives to regulate CO_2 hydrate formation. For instance, tetrahydrofuran (THF) enhances hydrate stability and facilitates CO_2 diffusion at the hydrate–liquid interface [18], while metal nanoparticles such as Cu, Fe, and Ag exhibit concentration-dependent effects, promoting hydrate growth at optimal loadings but inhibiting it at higher concentrations due to excessive Brownian motion, which disrupts the integrity of newly formed hydrate structures at the growth front through frequent collisions [19]. NBs have also been shown to significantly influence hydrate processes. During methane hydrate dissociation, the initial formation of NBs accelerates decomposition by alleviating mass transfer limitations, while additional NBs later in the process further promote hydrate collapse by shortening the diffusion path for methane molecules [20]. NBs also enhance hydrate nucleation and growth, likely by serving as preferential nucleation sites, as evidenced by their detection in dissociated water via nanoparticle tracking analysis and infrared spectroscopy. High concentrations of NBs have been associated with faster hydrate film formation, demonstrating their role in the hydrate memory effect [21]. In addition, the hydrophilic or hydrophobic properties of additives influence local gas concentrations near interfaces, further affecting hydrate formation [22].

While previous studies have provided valuable insights into CO_2 hydrate formation and the effects of chemical additives, they often fall short in capturing the complex molecular-level interactions that arise in the presence of NBs. NBs of hydrogen, nitrogen, and oxygen can be generated through various techniques and exhibit remarkable long-term stability in aqueous environments, especially in water, making them promising for a wide range of industrial applications. Furthermore, CO_2 NBs are of particular interest, not only for their ability to promote hydrate formation but also for their potential as a medium for greenhouse gas storage. Despite this promise, research exploring the role of NBs in gas hydrate processes remains limited, with most studies focusing on CO_2 NBs, particularly in methane-based host liquids [23,24]. Given the critical role of molecular interactions between novel additives and the hydrate phase, as well as the potential of nanobubble-enriched water to enhance CO_2 hydrate nucleation and growth, this study, for the first time, explores the influence of four types of NBs, i.e. hydrogen, nitrogen, oxygen, and carbon dioxide, on CO_2 hydrate formation and growth using a molecular-level approach. The investigation focuses on the effects of NB type, the combined impact of temperature and NBs, and the interactive influence of pressure and NBs on the kinetics of hydrate formation and growth. By leveraging advanced methodologies and incorporating diverse NB, this research aims to support the development of more efficient and promising strategies for CO_2 capture, an essential pillar of sustainable climate mitigation.

2. Theory and modelling

Computational nanoscience, particularly all-atom MD simulations, plays a pivotal role in elucidating the nucleation and growth of CO_2–water clathrates by providing detailed atomistic insights into the underlying molecular interactions. These simulations reveal nucleation pathways and growth mechanisms often inaccessible through experimental methods, thereby offering a deeper understanding of clathrate formation processes [25–27]. Furthermore, MD enables systematic investigation of the effects of temperature, pressure, and nanoscale additives on the kinetic behaviour of hydrates [13,28]. At its core, MD simulation numerically solves Newton's equations of motion to track the time evolution of each atom, where the trajectory of every atom is governed by its mass and the net force exerted upon it. These forces originate from interatomic potentials and any externally applied fields [29].

The reliability of MD simulations, including those for CO_2–water clathrate systems, depends critically on the accuracy of the employed force fields, which govern interatomic interactions and atomic trajectories. For CO_2–water clathrates, specialized models like TIP4P/Ice for water and the Extended Point Multipole (EPM) model for CO_2 are widely adopted due to their improved representation of key molecular interactions [30]. In this study, a hybrid force field approach was employed, using the TIP4P/Ice potential to model both intra- and intermolecular interactions of water, the EPM2 model for carbon dioxide, and a Lennard-Jones potential to describe interactions among the diatomic gases nitrogen, oxygen, and hydrogen, with the interaction coefficients of the atoms illustrated in Table 1. Cross-interactions between different atom types were computed using an arithmetic mixing rule. Bond lengths and angles within water, and the bonds of the dissolved gases, were constrained using the SHAKE algorithm, whereas the CO_2 molecular structure was maintained by allowing angular flexibility via a harmonic potential, ensuring accurate representation of its geometry. Long-range electrostatic interactions were treated using the particle–particle particle–mesh (PPPM) method, ensuring precise calculation of electrostatic forces across the system. All three Cartesian directions are subject to periodic boundary conditions.

Table 1
Interaction coefficients of atoms in water and gases.

Molecule	Elements	Epsilon (kcal/mol)	Sigma (Å)	Charge	Reference
Water	H	0	0	0.5897	[30]
	O	0.21084	3.1668	−1.1794	
Oxygen	O	0.09538	3.094	0	[42]
Nitrogen	N	0.07217	3.2973	0	[43]
Hydrogen	H	0.01988	2.720	0	[44]
Carbon dioxide	C	0.0559	2.757	0.6512	[45]
	O	0.1599	3.033	−0.3256	

A CO_2–water solution was prepared by randomly distributing 7015 water molecules and 1220 CO_2 molecules within a simulation cell measuring 6.8 × 6.03 × 7.3 nm. A hydrate seed, constructed as a 2 × 5 × 6-unit cell slab, was positioned at the center of the simulation box. The CO_2–water solution was subsequently placed on both sides of the hydrate seed, forming the surrounding solution phase. NBs containing equal mole fractions of four gases, CO_2, N_2, O_2, and H_2, were then incorporated into the CO_2–water system to establish the initial configuration of the nanobubble-enhanced model, as illustrated in Fig. 1. Each sample was equilibrated under the canonical (NVT) ensemble for 40 picoseconds (ps) with a 1 femtosecond (fs) timestep, including the hydrate seeds. Due to the memory effect, these seeds serve as pre-nucleation sites that accelerate hydrate formation and growth. The memory effect refers to the phenomenon whereby gas hydrates nucleate more readily or rapidly in water with a prior history of hydrate formation compared to fresh water without such history [31]. Thus, even if hydrate structures are disrupted during the NVT equilibration, the presence of seeds continues to facilitate hydrate formation, allowing researchers to effectively study the influence of nano additives on hydrate nucleation and growth. Subsequently, samples were subjected to the isothermal–isobaric (NPT) ensemble under desired thermodynamic conditions for at least 85 nanoseconds (ns) to investigate the effects of different types of NBs, as well as the combined influences of NBs with temperature and pressure on clathrate hydrate formation and growth. All simulations were performed using the open-source LAMMPS package [32], visualized with OVITO [33], and clathrate formation analyzed using the open-source GRADE code after processing the trajectories with a custom-developed script for compatibility [34].

3. Results and discussion

3.1. Effects of nanobubble type

In the development of carbon capture, utilization, and storage (CCUS) technologies, the formation of CO_2 hydrates represents a promising approach for long-term CO_2 sequestration. CO_2 hydrate is a non-stoichiometric, ice-like crystalline compound formed under conditions of high pressure and low temperature, in which CO_2 molecules are trapped within a hydrogen-bonded network of water molecules. Among the various hydrate structures, the most prevalent is structure I (sI) CO_2 hydrate. Each unit cell of sI hydrate contains two types of cavities: six large cages ($6\times6^2 5^{12}$) and two small cages (2×5^{12}). These cages, stabilized by the water lattice, act as hosts for CO_2 guest molecules. Given the molecular size of CO_2 (approximately 5.12 Å), it can be accommodated not only in the large ($5^{12}6^2$) and small (5^{12}) cages of the sI hydrate but also in the small cages of structure II (sII), the small and medium ($4^3 5^6 6^3$) cages of structure H (sH), and the small cages in semi-clathrate hydrates [7,35]. The number of the two dominant formed cages, $5^1 2^2$ and $6^2 5^1 2^2$, along with the total number of these cages during the initial stage at 28.35 ns is shown in Fig. 2a for the water–gas sample without a NB (WG), as well as for samples containing NBs of carbon dioxide (CDNB), oxygen (ONB), nitrogen (NNB), and hydrogen (HNB) at 2 MPa and 260 K. The temporal evolution of the $5^1 2^2$ cages, $6^2 5^1 2^2$ cages, and the total number of formed cages over time is also presented in Fig. 2b, c, and d, respectively. As illustrated in Fig. 2d, by 85 ns, all nanobubbled samples exhibited a higher total number of formed cages compared to the non-nanobubbled sample, with the HNB sample showing the highest overall formation, followed by NNB, ONB, and CDNB. A closer analysis of Fig. 2d reveals that the enhancement in cage formation due to ONB, NNB, and HNB emerges earlier, whereas the impact of CDNB becomes pronounced only after approximately 60 ns. This delayed response suggests a lag in the structural influence of CDNB on hydrate growth. Further insights from Fig. 2a, focusing on the initial stage at 28.35 ns, shows that the presence of NBs, including CDNB, promotes the formation of large cages ($6^2 5^{12}$). However, the number of small cages (5^{12}) in the CDNB system is notably lower compared to the NNB and HNB samples.

Analysis of non-nanobubbled aqueous CO_2 samples reveals that, over time, CO_2 molecules tend to self-associate within the bulk solution, forming dispersed molecular clusters. As illustrated in Fig. 3a, three distinct clusters are observed at 28.35 ns. These clusters appear to induce a local reorganization of surrounding water molecules into more ordered hydrogen-bonding networks, thereby facilitating the formation of clathrate cages. This observation supports the hypothesis that molecular aggregation enhances local structural order and plays a key role in initiating phase transformation. From the perspective of several nucleation theories, the formation of CO_2 hydrate is driven by the ordered arrangement of water molecules and the localized ordering of gas molecules. This concept is specifically emphasized in both the labile cluster nucleation hypothesis and the local structuring nucleation theory. MD studies on CO_2 hydrate formation have introduced the blob nucleation mechanism, which proposes that guest molecules initially concentrate into dense regions (blobs) that are in equilibrium with the surrounding solution. These blobs then induce the formation of water cages, giving rise to a clathrate nucleus. This mechanism integrates key elements of both the local structuring and labile cluster hypotheses [7,36].

In contrast, hydrogen-, oxygen-, and nitrogen-nanobubbled samples show no evidence of pure CO_2 clustering in the bulk solution. Instead, due to the pronounced hydrophobicity of these gases, CO_2 molecules preferentially migrate toward and adsorb onto the NB surfaces, as depicted in Fig. 3b-e. These hydrophobic surfaces act as accelerator spots that promote concentration gradients and enhance the kinetics of clathrate formation. More importantly, their presence not only drives CO_2 accumulation at well-defined interfacial regions but also reduces the likelihood of random, spontaneous nucleation events in the bulk

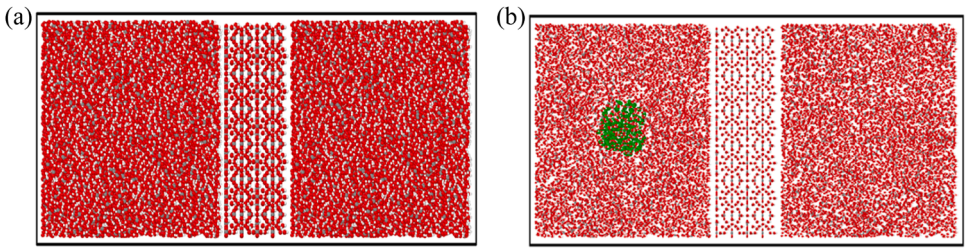

Fig. 1. Initial configuration of (a) a non-nanobubble and (b) a nanobubble-containing water–carbon dioxide sample, including a hydrate seed.

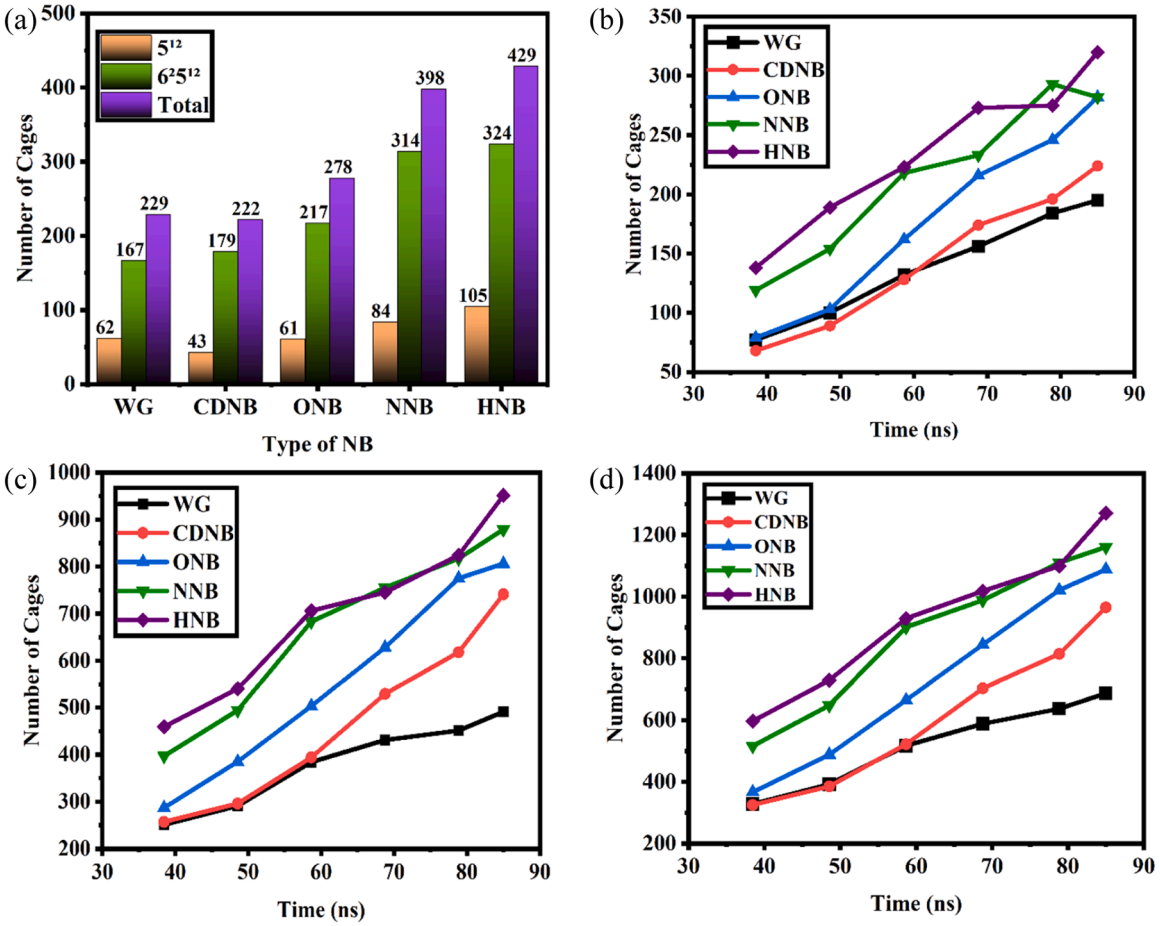

Fig. 2. Number of formed hydrate cages: (a) small, large, and total cages at 28.35 ns; (b) small cages, (c) large cages, and (d) total cages over the course of 85 ns at 2 MPa and 260 K.

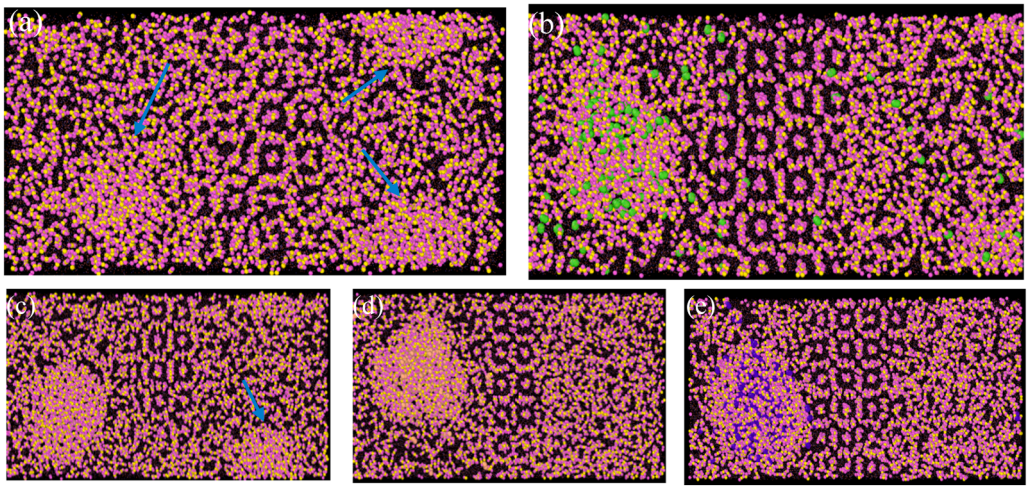

Fig. 3. Snapshots of (a) WG, (b) HNB with diffused hydrogen atoms (green) in the solution, (c) CDNB, (d) ONB, and (e) NNB samples at 28.35 ns at 2 MPa and 260 K.

solution. By guiding CO_2 molecules toward energetically favorable aggregation sites, the system minimizes stochasticity in both spatial and temporal aspects of nucleation, resulting in a more directed and efficient clathrate formation process. Interestingly, CO_2-nanobubbled (CDNB) samples exhibit a hybrid behaviour. In addition to CO_2 molecules adsorbed at the nanobubble interfaces, dispersed CO_2 clusters are also observed within the bulk solution, as shown in Fig. 3c. This dual behaviour is likely due to CO_2's relatively lower hydrophobicity compared to hydrogen, nitrogen, and oxygen, which allows more CO_2 molecules to remain dissolved in the aqueous phase than in other nanobubble-containing samples. As illustrated in Fig. 2a, the number of large cages formed shows a decreasing trend from HNB to NNB, followed by ONB, and finally CDNB. This pattern can be attributed to differences in the hydrophobicity of the NB gases. Hydrogen and nitrogen, being more hydrophobic than oxygen and carbon dioxide, drive a greater number of CO_2 molecules to rapidly adsorb onto their nanobubble

surfaces during the early stages. This adsorption generates a steeper concentration gradient and promotes the formation of larger CO_2-rich blobs, which enhance local water structuring and facilitate clathrate formation. In comparison to the WG sample, the CDNB sample allows a portion of CO_2 molecules to adsorb onto the nanobubble surfaces. As a result, more water molecules remain available in the bulk solution for the remaining CO_2, which generally tends to form larger hydrate cages. This leads to a higher number of large cages in the CDNB sample compared to the WG sample.

At the early stage of the hydration process, as illustrated in Fig. 2a, the number of small cages formed in the HNB and NNB samples is significantly higher than in the other samples, suggesting that additional mechanisms may also contribute to hydrate formation. As previously discussed, dissolved CO_2 molecules tend to adsorb onto the surfaces of these NBs. However, due to the small molecular size of hydrogen and nitrogen, a limited number of these gas molecules can diffuse, or "breathe", into the solution from the NB core. The presence of small-molecule gases such as H_2 and N_2 has been reported in an experimental study to significantly enhance the CO_2 hydrate formation process. Specifically, hydrogen was found to influence the initial morphology of CO_2 hydrate films. Raman spectroscopy results further revealed that the presence of hydrogen produced a looser hydrate film structure, which improved mass transfer and supported the continued growth of the hydrate layer. Similarly, nitrogen has been shown to play a comparable role; however, its participation in mixed CO_2/N_2 hydrate formation induces adaptive changes in the film's growth behaviour [37]. A similarly loose hydrate structure has also been reported in molecular dynamics simulations of CO_2 hydrates confined within porous media [38,39]. In addition, the presence of small guest molecules such as H_2 and N_2 promotes the formation of small hydrate cages during the early stages of hydrate growth. In contrast, this mechanism is absent in CDNB samples. In the CDNB system, hydrate formation initially favors the development and growth of larger cages. However, as the system becomes more structurally organized and thermodynamically favorable over time, the formation of smaller cages is progressively enhanced. This delayed but sustained nucleation ultimately leads to a continuous increase in the total number of hydrate cages formed in the CDNB sample than WG sample.

The four-body order parameter, commonly denoted as F_4, is a valuable tool in molecular dynamics simulations for characterizing the local structural arrangement of water molecules, particularly during clathrate hydrate formation. It is especially effective in distinguishing between water molecules that participate in the formation of hydrate cages and those that remain in bulk liquid water. By quantifying the degree of local structural ordering within the water network, the F_4 parameter offers important insights into the nucleation and growth mechanisms of CO_2 hydrates. As a classical order parameter, F_4 is defined by the following equation, and its theoretical values range from approximately −0.4–0.7. In this range, typical values for the ice, liquid water, and hydrate phases are around −0.4, −0.04, and 0.7, respectively [35].

$$F_4 = \frac{1}{n}\sum_{i=1}^{n}\cos 3\varphi_i \quad (1)$$

where φ_i represents the dihedral angle formed between the oxygen atoms of two adjacent water molecules and their outermost hydrogen atoms, while n denotes the number of oxygen atoms pairs between H_2O molecules within a distance of 0.35 nm.

Fig. 4 illustrates the F_4 parameter for the water–gas sample without NBs and for samples containing various NBs. Over time, the F_4 values of the nanobubbled samples consistently exceeded those of the pure water–gas sample, indicating that NBs promote the nucleation and growth of CO_2 hydrate at 260 K and 2 MPa. Notably, from the initial stage at 28.35 ns, samples containing the more hydrophobic diatomic gases exhibited higher F_4 values compared to the non-nanobubbled sample, suggesting enhanced local structural ordering around water

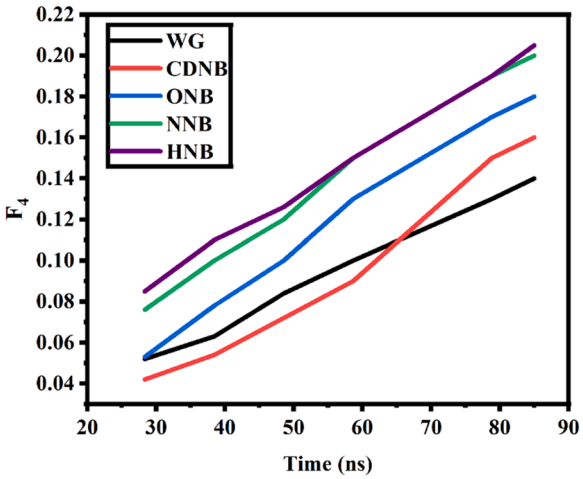

Fig. 4. Four-order structural parameter of various samples.

molecules. A closer examination reveals that during the initial and intermediate stages, the F_4 parameter of the non-nanobubbled sample remained higher than that of the CDNB sample. This indicates that the presence of CDNB initially inhibits hydrate nucleation, likely due to the reduced formation of small $5^{1}2$ cages in this sample, as previously discussed. However, as time progresses and structural ordering improves, the conditions become more favorable for the formation of small cages. Consequently, the CDNB system overcomes its initial lag and ultimately enhances CO_2 hydrate growth.

Potential energy is commonly used as an indicator of structural transitions, such as hydrate growth or dissociation. Under constant temperature conditions, the average kinetic energy of the sample remains stable. Consequently, changes in the total energy primarily reflect variations in potential energy, which arise from interatomic interactions, including van der Waals forces, electrostatic interactions, and hydrogen bonding. During hydrate formation, water and gas molecules reorganize into an energetically favorable, crystalline structure composed of host water cages enclosing guest gas molecules. This transition to a more ordered phase is exothermic, leading to a net decrease in the sample's potential energy. As a result, a downward trend in potential energy over time is often interpreted as a clear signature of hydrate nucleation and growth, indicating increased structural stabilization of the sample [40].

The variation in potential energy for the different samples is illustrated in Fig. 5. It is evident that the addition of NBs significantly alters the potential energy profile compared to the pure water–gas sample.

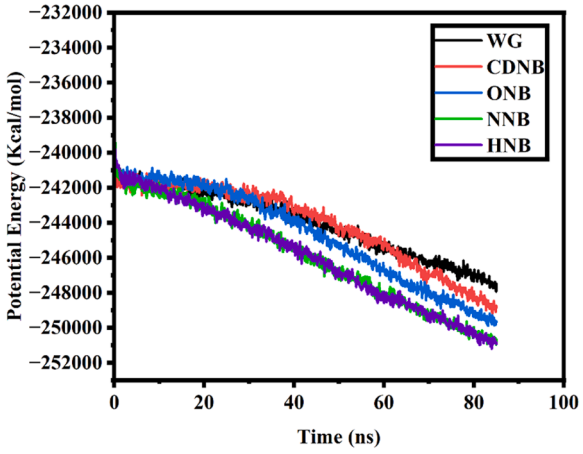

Fig. 5. Temporal evolution of potential energy for the pure water–gas sample (WG) and nanobubbled samples (CDNB, ONB, NNB, and HNB).

Specifically, samples with higher NB surface hydrophobicity exhibit a more rapid decline in potential energy, indicating that increased hydrophobicity enhances the exothermic nature of hydrate formation. This behavior suggests that NBs actively promote and accelerate hydrate nucleation and growth. To quantify the rate of hydrate formation, the slope of the potential energy curve was determined through linear fitting, with results presented in Table 2. The data reveal that hydrogen and nitrogen NB samples, which possess higher surface hydrophobicity, exhibit the steepest energy decline, reflecting faster hydrate formation. This enhancement is attributed to favorable gas aggregation and structural ordering at the hydrophobic NB interfaces. As previously discussed, the CDNB sample shows a delayed onset of hydrate promotion during the early stages. However, as the simulation progresses, the sample becomes increasingly ordered, with enhanced hydrogen bonding, ultimately promoting hydrate formation at later times.

It is generally anticipated that, upon complete hydrate formation, the sample's potential energy would reach a plateau indicative of a fully converted, energetically minimized hydrate structure. However, in the present simulations, the potential energy profiles do not completely level off, indicating that a fraction of water molecules remains in the non-hydrated state. This outcome is unsurprising, given the large size of the simulated samples using the all-atom approach and the limited duration of accessible simulation timescales. Full conversion of all water molecules to hydrate likely requires microsecond timescales or longer, well beyond the nanosecond scale employed in this study. Nevertheless, the comparative analysis presented here provides valuable insights into the underlying mechanisms of hydrate formation and highlights the influence of NB properties on nucleation behaviour. These findings contribute to a deeper molecular-level understanding of hydrate nucleation and growth pathways. Such insights are essential for a better understanding of the hydrate process, for advancing hydrate-based technologies in carbon capture and storage, and for optimizing hydrate formation and inhibition strategies.

3.2. Impacts of temperature and nanobubble

To investigate the dual impact of NBs and temperature on CO_2 hydrate formation, three samples, HNB, CDNB, and WG, were analyzed at a pressure of 2 MPa and temperatures of 240 K and 260 K. The temporal evolution of the two dominant hydrate cages, $5^1 2$ and $6^2 5^1 2$, the total number of formed cages over time at 240 K, and the comparison of total cage formation at both temperatures at 85 ns are presented in Fig. 6a, b, c, and d, respectively. As shown in Fig. 6c, by 85 ns, the nanobubble-containing samples exhibited a higher total number of formed cages compared to the non-nanobubbled sample at 240 K. However, Fig. 6d reveals that at 260 K, the presence of NBs has an even greater effect on cage formation than at 240 K. Additionally, the cage formation process at 260 K appears to be more sensitive to the type of NB, as the number of formed cages in the presence of HNB is significantly higher than in the presence of CDNB. In contrast, at 240 K, the samples are less sensitive to the type of NB, particularly in the formation of $5^1 2$ cages, as shown in Fig. 6a, since there is only a small difference in the total number of formed cages between the HNB and CDNB samples. A comparison of Figs. 2c and 6c, which illustrate the total number of cages formed over time at 260 K and 240 K, respectively, reveals distinct differences in hydrate formation dynamics. At 260 K, cage formation exhibits a continuous and steady increase throughout the simulation, indicating a stable growth process. In contrast, the trend at 240 K is notably less consistent. For instance, in the CDNB sample, a decline in the total number of cages is observed around 80 ns, followed by a subsequent recovery. This fluctuation suggests that cage formation at 240 K is comparatively less consistent and more prone to disruption than at 260 K.

Table 2
Linear fit slopes of potential energy evolution for nanobubbled and non-nanobubbled samples.

Sample	WG	CDNB	ONB	NNB	HNB
Slope	-77.19	-89.77	-111.81	-118.40	-119.80

As previously discussed, at 260 K and 2 MPa, the formation of blob-like structures was observed in the WG sample. While nanobubbled samples benefited from the hydrophobic surfaces of the NBs, which acted as catalytic interfaces, reducing the stochastic nature of blob nucleation in both space and time, thereby promoting CO_2 hydrate formation. Additionally, HNB was found to further enhance cage formation through a "breathing" mechanism, wherein dynamic gas exchange between the NB and the surrounding solution facilitates hydrate cage formation. All of these enhancement mechanisms are strongly dependent on atomic mobility. As the temperature decreases, atomic motion becomes increasingly restricted, limiting the activation of these mechanisms. For instance, at 240 K, the cage formation process showed reduced sensitivity to the type of NB and its surface hydrophobicity. As CO_2 molecules preferentially migrate and aggregate at more hydrophobic interfaces, sufficient mobility, which is more restricted at lower temperatures, is required for this behaviour to occur. As a result, the influence of NB type on hydrate formation becomes less pronounced at 240 K compared to 260 K.

The Radial Distribution Function (RDF) offers valuable insights into the spatial arrangement of particles by quantifying the probability of finding a particle at a specific distance from a reference particle. It can be calculated using the following equation [41]:

$$x_\upsilon x_\xi \rho g_{\upsilon\xi}(r) = \frac{1}{N}\left\langle \sum_{i=1}^{N_\upsilon}\sum_{i=1}^{N_\xi}\delta(r + r_i - r_j)\right\rangle \quad (2)$$

where x, ρ, $g(r)$, N, υ, and ξ represent mole fraction, density, RDF, the number of total atoms, and the types of chemicals, respectively. Fig. 7a presents the RDF between hydrogen and dissolved CO_2 at two temperatures, i.e. 240 K and 260 K, evaluated at 39.06 ns, representing a mid-stage of hydrate growth where the sample has dynamically evolved and is poised for further structural development. The RDF at 260 K exhibits a more pronounced peak compared to that at 240 K, indicating a higher probability of finding CO_2 molecules around hydrogen atoms. This suggests that CO_2 molecules are more favorably positioned near hydrogen at 260 K. Furthermore, Fig. 7b shows the RDF between hydrogen and water at these two temperatures. The hydrogen–water RDF at 260 K displays a higher peak than at 240 K, indicating more interaction between hydrogen and water at the higher temperature. This enhanced "breathing" mechanism at 260 K suggests increased molecular mobility, further confirming that reduced mobility at lower temperatures can limit interaction and hinder the hydrate formation process. These observations highlight the significance of temperature in hydrate nucleation and growth. Specifically, 260 K appears to offer more favorable conditions, under the given pressure, for promoting hydrate formation due to an optimal balance between molecular mobility and intermolecular interactions. However, further increases in temperature may disrupt this balance, as enhanced atomic motion can overcome hydrogen bonding and other intermolecular forces, ultimately inhibiting cage formation. This underscores the existence of an optimal thermodynamic window for hydrate formation, where both molecular mobility and interaction strength are well balanced.

As observed at 240 K, hydrate formation appears to be less sensitive to the hydrophobicity of NBs. Notably, the number of formed cages in the presence of CDNB is slightly higher than in other samples at this temperature, as illustrated in Fig. 6d. A comparison of the cage formation trends at 240 K and 260 K (Figs. 2d and 6c), reveals distinct differences in growth behaviour. At 260 K, cage formation shows a continuous and steady increase over time, indicating a stable and sustained growth process. In contrast, at 240 K, the trend is less consistent. Specifically, in the CDNB sample, the total number of formed cages decreases between 68.75 ns and 78.85 ns before partially recovering,

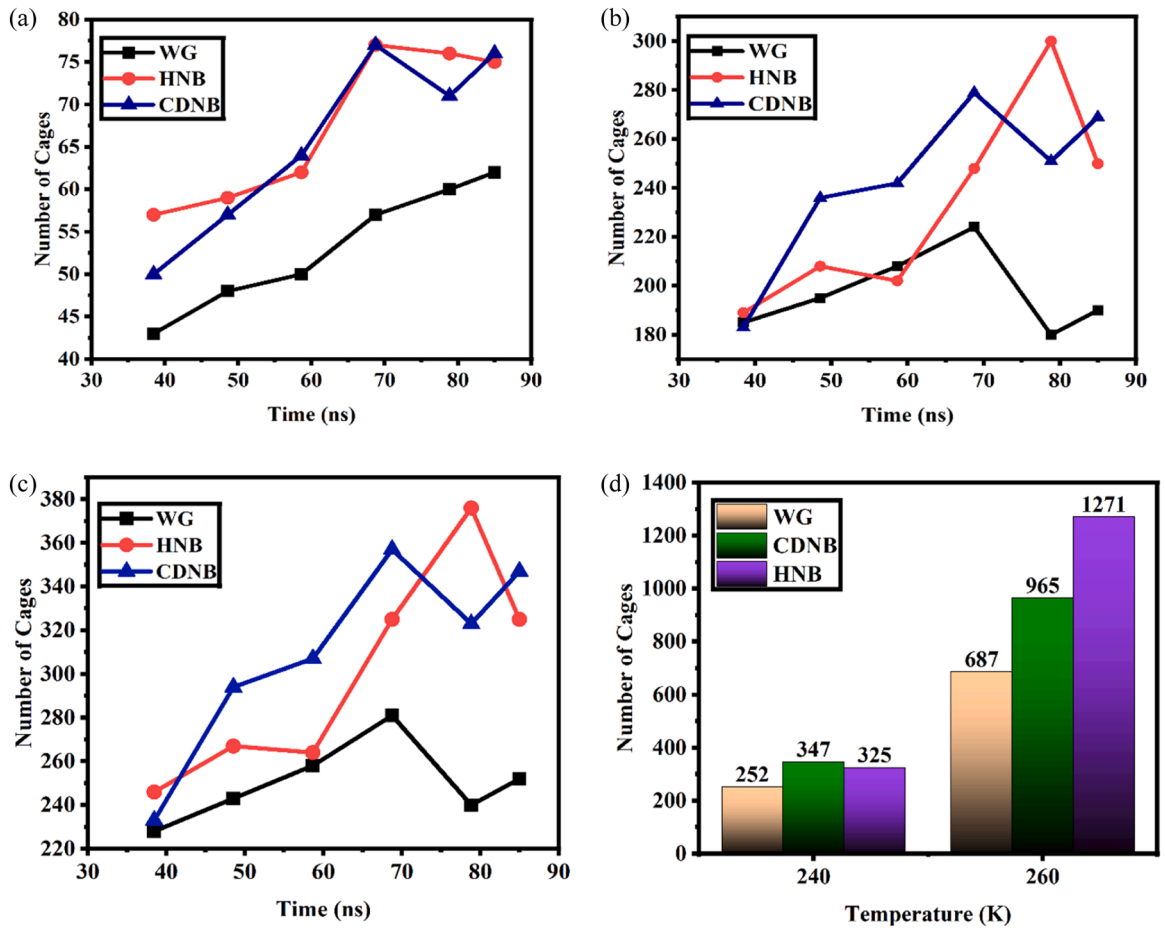

Fig. 6. Number of formed hydrate cages: (a) small, (b) large, and (c) total cages over time at 2 MPa and 240 K; (d) comparison of the number of formed cages at 85 ns between 240 K and 260 K at 2 MPa.

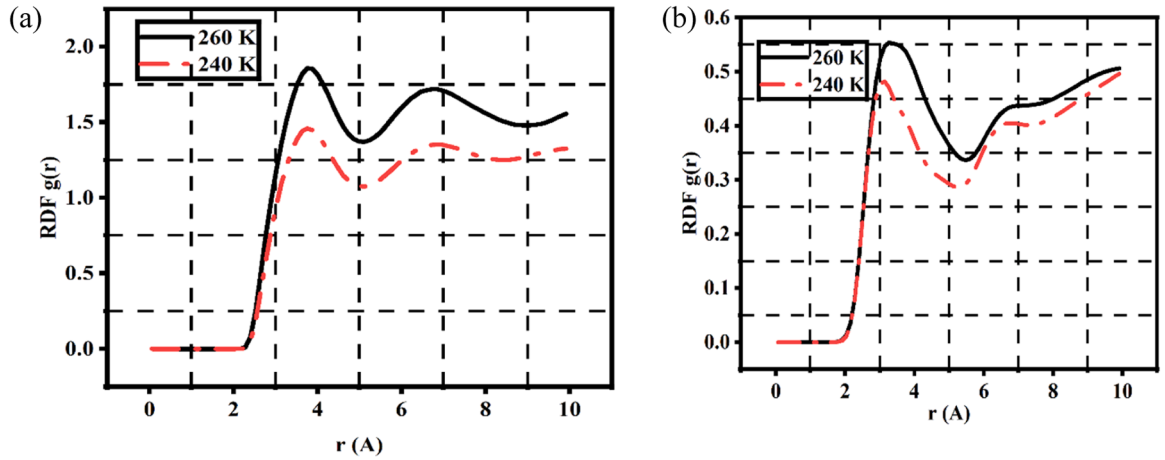

Fig. 7. RDF of (a) hydrogen–carbon dioxide and (b) hydrogen–water in the HNB sample at 39.06 ns.

suggesting unstable growth dynamics at the lower temperature. Further comparison of the F_4 parameter for CDNB samples at both temperatures (Fig. 8a), reveals that at 240 K, the F_4 value increases within the same time window (68.75–78.85 ns) as at 260 K. To better understand this behavior, the total number of formed rings and cups, fundamental structural units in hydrate formation, was examined. Initially, rings are formed between water molecules, followed by their assembly into cups. The combination of these cups ultimately results in the formation of complete hydrate cages. This suggests that the rise in the F_4 parameter at 240 K is primarily due to the accumulation of these substructures (Fig. 8b), which fail to complete the cage architecture under kinetically limited conditions. The inability of cups and rings to transition into complete cages at 240 K is likely due to kinetic hindrance, which disrupts stable cage growth. Some partially formed cages may even revert back to cup structures due to discontinuous growth. In contrast, at 260 K, the system overcomes this kinetic barrier more effectively, allowing cups to convert more readily into fully formed cages. These findings highlight the existence of an optimal kinetic and

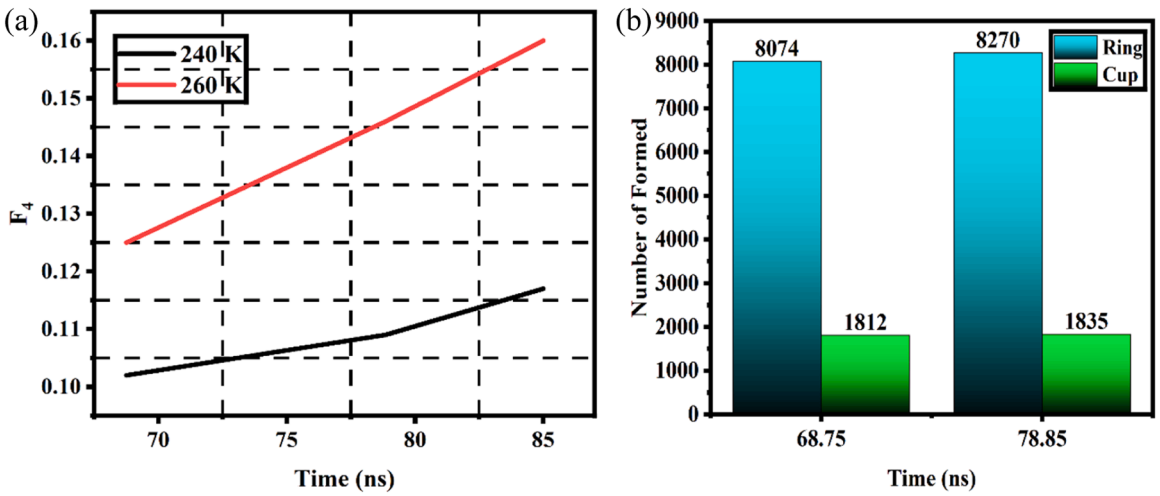

Fig. 8. (a) F_4 parameter of CDNB at two different temperature and (b)the number of total formed rings and cages at 240 K for CDNB at two different times.

thermodynamic window for hydrate formation, where both molecular mobility and interaction strength are balanced to support sustained cage growth.

3.3. *Influences of pressure and nanobubble*

The influence of pressure and the presence of NBs on CO_2 hydrate formation investigated using three distinct samples. WG served as the nanobubble-free reference, while CDNB and HNB represented nanobubble-containing samples, all studied under conditions of 10 MPa and 260 K. The temporal evolution of the two dominant hydrate cages, $5^1 2$ and $6^2 5^1 2$, as well as the total number of cages formed over time at 10 MPa and 260 K, are illustrated in Fig. 9a, b, and c, respectively. As illustrated in Fig. 9c, after 85 ns, the total number of formed cages in the HNB sample is slightly higher than in the WG sample. Notably, in contrast to the results at lower pressure (2 MPa), shown in Fig. 2d, the total number of formed cages in the CDNB sample is lower than in the nanobubble-free WG sample. This behaviour indicates the dual role of NBs, which can act as both promoters and inhibitors of hydrate formation [23].

Increasing the pressure in both nanobubbled and non-nanobubbled samples results in higher sample density and stronger molecular interactions. In the non-nanobubbled sample, this pressure-induced densification enhances interactions between molecules, especially between water molecules, creating a more favorable environment for hydrate nucleation, particularly for the formation of small $5^1 2$ cages. In contrast, in samples containing-nanobubble samples, the increased pressure also densifies the nanobubble itself, intensifying molecular interactions within it. This behaviour reduces the availability of active interaction sites at the gas–liquid interface, particularly on the nanobubble surface, which typically plays a catalytic role in organizing the local molecular structure for hydrate formation, as previously discussed. Interestingly, the presence of carbon dioxide nanobubble significantly reduces the formation of hydrate cages at elevated pressures. At lower pressures, the intermolecular interactions between solution molecules, particularly water–water and water–CO_2, are relatively weak and insufficient to induce the local structural ordering required for hydrate nucleation. In this regime, the presence of a CDNB plays a beneficial role by providing a gas–liquid interface that helps organize water molecules into more ordered, hydrogen-bonded structures, effectively lowering the growth barrier for hydrate cages. However, as pressure increases, the intensified molecular interactions between CO_2 and water in the bulk become strong enough to promote local ordering and hydrate formation without the need for interfacial assistance. In this high-pressure regime, the role of the CDNB shifts. Instead of promoting structural order, the NB becomes disruptive. It introduces disorder, potentially disturbing the hydrogen-bond network formed through enhanced bulk interactions, a network that would otherwise facilitate hydrate cage formation. As a result, at higher pressures, the NB no longer serves as a catalytic site for atomic structure ordering but instead acts as a structural obstacle, impeding hydrate formation. Furthermore, at lower pressure, the presence of HNB (Fig. 2d) significantly enhances hydrate cage formation compared to non-nanobubbled samples, indicating a strong promotive effect. However, as pressure increases, this effect diminishes, and the difference in the number of formed cages between hydrogen nanobubbled and non-nanobubbled samples becomes much less pronounced. These observations underscore a pressure-dependent shift in the dominant mechanism of hydrate nucleation, from nanobubble-induced

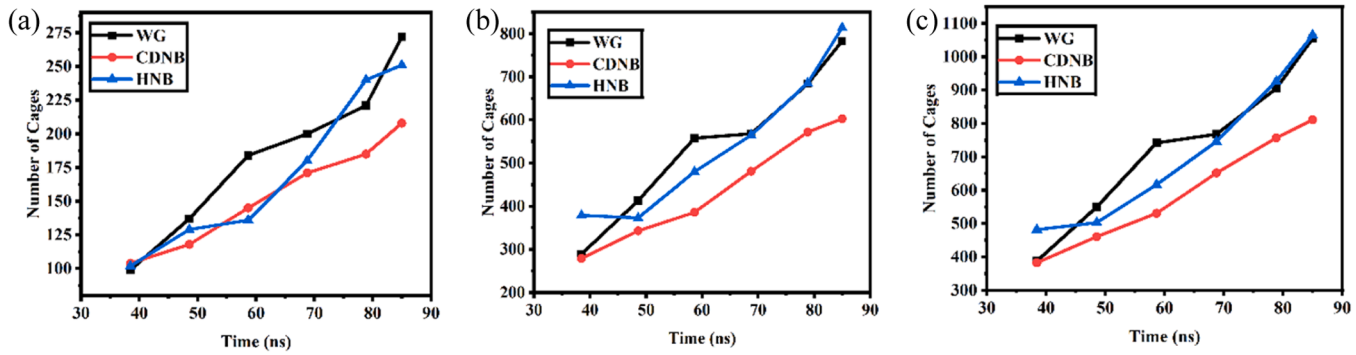

Fig. 9. The number of formed hydrate cages: (a) small, (b) large, and (c) total cages at 10 MPa and 260 K.

ordering at low pressure to bulk interaction- driven ordering at high pressure.

4. Conclusion

This study utilizes molecular dynamics (MD) simulations to investigate the effects of various nanobubbles (NBs), namely nitrogen, oxygen, hydrogen, and carbon dioxide, on CO_2 hydrate formation under diverse thermodynamic conditions. The results at 2 MPa and 260 K reveal that under optimal thermodynamic conditions, the hydrophobic surfaces of NBs act as nucleation spots, attracting CO_2 molecules and enhancing local concentration gradients. This interfacial accumulation not only accelerates hydrate formation kinetics but also reduces the occurrence of stochastic nucleation events in the bulk phase, leading to more efficient and directed clathrate growth. Furthermore, the diffusion of small guest molecules such as H_2 and N_2 from the NB core further enhances the formation of hydrate cages. However, this enhancement is highly dependent on molecular mobility; under sub-optimal conditions, particularly at a lower temperature (240 K), restricted atomic motion suppresses these mechanisms, diminishing the influence of NB type and surface characteristics. A pressure-dependent dual role of NBs is also observed when the system pressure increases from 2 MPa to 10 MPa. While CO_2 NBs promote hydrate formation at optimal pressures by inducing local structural ordering, they become disruptive at higher pressures. In this regime, strong bulk molecular interactions dominate hydrate nucleation, while the presence of carbon dioxide NBs introduces disorder that hinders, rather than promotes, cage formation.

CRediT authorship contribution statement

Xinyan Wang: Writing – review & editing, Supervision, Project administration, Funding acquisition. **Hamidreza Hassanloo:** Writing – review & editing, Writing – original draft, Visualization, Software, Methodology, Formal analysis, Conceptualization.

Declaration of Competing Interest

There is no conflict of interest to declare.

Acknowledgement

This work was supported by a UKRI Future Leaders Fellowship (MR/T042915/1 and UKRI1057) and EPSRC DTP (EP/T518116/1–2688449). MD simulations were run on MMM Hub Young, the UK's National Supercomputing Service.

Data availability

Data will be made available on request.

References

[1] S.A. Rackley, Carbon Capture and Storage, Butterworth-Heinemann, 2017.
[2] G. Pandey, T. Poothia, A. Kumar, Hydrate based carbon capture and sequestration (HBCCS): an innovative approach towards decarbonization, Appl. Energy 326 (2022) 119900.
[3] M.-T. Huang, P.-M. Zhai, Achieving Paris Agreement temperature goals requires carbon neutrality by middle century with far-reaching transitions in the whole society, Adv. Clim. Change Res. 12 (2) (2021) 281–286.
[4] D.Y. Shu, S. Deutz, B.A. Winter, N. Baumgärtner, L. Leenders, A. Bardow, The role of carbon capture and storage to achieve net-zero energy systems: trade-offs between economics and the environment, Renew. Sustain. Energy Rev. 178 (2023) 113246.
[5] B. Peachey, N. Maeda, Challenging the chemistry of climate change, Chemistry 6 (6) (2024) *2624–8549*.
[6] Q. Sun, Y.T. Kang, Review on CO2 hydrate formation/dissociation and its cold energy application, Renew. Sustain. Energy Rev. 62 (2016) 478–494.
[7] F.-P. Liu, A.-R. Li, S.-L. Qing, Z.-D. Luo, Y.-L. Ma, Formation kinetics, mechanism of CO2 hydrate and its applications, Renew. Sustain. Energy Rev. 159 (2022) 112221.
[8] J.A. Ripmeester, S. Alavi, Some current challenges in clathrate hydrate science: nucleation, decomposition and the memory effect, Curr. Opin. Solid State Mater. Sci. 20 (6) (2016) 344–351.
[9] Y. Zhang, L. Zhao, S. Deng, R. Zhao, X. Nie, Y. Liu, Effect of nanobubble evolution on hydrate process: a review, J. Therm. Sci. 28 (2019) 948–961.
[10] M. Aminnaji, et al., CO2 Gas hydrate for carbon capture and storage applications–Part 1, Energy (2024) 131579.
[11] H. Hassanloo, X. Wang, Combustion mechanism of nanobubbled dodecane: a reactive molecular study, Fuel 374 (2024) 132486.
[12] P. Pal, A. Kioka, S. Maurya, R.-A. Doong, Innovative nanobubble technology: fuelling the future of bioenergy and carbon mitigation, Renew. Sustain. Energy Rev. 209 (2025) 115118.
[13] X. Zhang, et al., Research progress of molecular dynamics simulation on the formation-decomposition mechanism and stability of CO2 hydrate in porous media: a review, Renew. Sustain. Energy Rev. 167 (2022) 112820.
[14] K. Lijith, R.S. Rao, D.N. Singh, Detection of formation and dissociation of CO2 hydrates in fine-sands through acoustic waves, Fuel 357 (2024) 129802.
[15] L. Chen, H. Lu, J.A. Ripmeester, Raman spectroscopic study of CO2 in hydrate cages, Chem. Eng. Sci. 138 (2015) 706–711.
[16] S. Almenningen, J. Gauteplass, P. Fotland, G.L. Aastveit, T. Barth, G. Ersland, Visualization of hydrate formation during CO2 storage in water-saturated sandstone, Int. J. Greenh. Gas. Control 79 (2018) 272–278.
[17] M. Takahashi, T. Kawamura, Y. Yamamoto, H. Ohnari, S. Himuro, H. Shakutsui, Effect of shrinking microbubble on gas hydrate formation, J. Phys. Chem. B 107 (10) (2003) 2171–2173.
[18] A. Phan, H. Schlösser, A. Striolo, Molecular mechanisms by which tetrahydrofuran affects CO2 hydrate Growth: implications for carbon storage, Chem. Eng. J. 418 (2021) 129423.
[19] N. Liu, H. Zhu, J. Zhou, L. Yang, D. Liu, Molecular dynamics simulations on formation of CO2 hydrate in the presence of metal particles, J. Mol. Liq. 331 (2021) 115793.
[20] Y. Lu, et al., A molecular dynamics study on nanobubble formation and dynamics via methane hydrate dissociation, Fuel 341 (2023) 127650.
[21] Y. Feng, et al., Study of hydrate nucleation and growth aided by micro-nanobubbles: probing the hydrate memory effect, Energy 290 (2024) 130228.
[22] Z. He, F. Mi, F. Ning, Molecular insights into CO2 hydrate formation in the presence of hydrophilic and hydrophobic solid surfaces, Energy 234 (2021) 121260.
[23] M. Pan, P. Naeiji, N.J. English, Study of CO2-hydrate formation in contact with bulk nanobubbles: an investigation from experiment and molecular-dynamics simulations, J. Colloid Interface Sci. 685 (2025) 415–426.
[24] B. Fang, et al., Effects of nanobubbles on methane hydrate dissociation: a molecular simulation study, Fuel 345 (2023) 128230.
[25] S. Sinehbaghizadeh, A. Saptoro, S. Amjad-Iranagh, P. Naeiji, A.N.T. Tiong, A. H. Mohammadi, A comprehensive review on molecular dynamics simulation studies of phenomena and characteristics associated with clathrate hydrates, Fuel 338 (2023) 127201.
[26] B.C. Barnes, A.K. Sum, Advances in molecular simulations of clathrate hydrates, Curr. Opin. Chem. Eng. 2 (2) (2013) 184–190.
[27] S. Das, K.M. Tadepalli, S. Roy, R. Kumar, A review of clathrate hydrate nucleation, growth and decomposition studied using molecular dynamics simulation, J. Mol. Liq. 348 (2022) 118025.
[28] N. Liu, T. Li, T. Liu, L. Yang, Molecular dynamics simulations of the effects of metal nanoparticles on methane hydrate formation, J. Mol. Liq. 356 (2022) 118962.
[29] A. Satoh, Introduction to practice of molecular simulation: molecular dynamics, Monte Carlo, Brownian dynamics. Lattice Boltzmann and dissipative particle dynamics, Elsevier, 2010.
[30] A. Guerra, S. Mathews, J.T. Su, M. Marić, P. Servio, A.D. Rey, Molecular dynamics predictions of transport properties for carbon dioxide hydrates under pre-nucleation conditions using TIP4P/Ice water and EPM2, TraPPE, and Zhang carbon dioxide potentials, J. Mol. Liq. 379 (2023) 121674.
[31] Y. Wei, N. Maeda, Mechanisms of the memory effect of clathrate hydrates, Chem. Eng. Sci. 270 (2023) 118538.
[32] S. Plimpton, Fast parallel algorithms for short-range molecular dynamics, J. Comput. Phys. 117 (1) (1995) 1–19.
[33] A. Stukowski, Visualization and analysis of atomistic simulation data with OVITO–the Open Visualization Tool, Model. Simul. Mater. Sci. Eng. 18 (1) (2009) 015012.
[34] F. Mahmoudinobar, C.L. Dias, GRADE: a code to determine clathrate hydrate structures, Comput. Phys. Commun. 244 (2019) 385–391.
[35] X. Jing, Q. Luo, X. Cui, Q. Wang, Y. Liu, Z. Fu, Molecular dynamics simulation of CO2 hydrate growth in salt water, J. Mol. Liq. 366 (2022) 120237.
[36] M. Aminnaji, et al., CO2 Gas hydrate for carbon capture and storage applications–Part 1, Energy 300 (2024) 131579.
[37] Y. Xie, et al., Effects of H2/N2 on CO2 hydrate film growth: morphology and microstructure, Chem. Eng. J. 431 (2022) 134004.
[38] X. Zhang, T. Shan, H. Song, J. Li, Q. Wu, Molecular dynamics study of the micro-mechanism of CO2 hydrate formation in the confined space of porous media, Int. J. Heat. Mass Transf. 244 (2025) 126940.
[39] X. Zhang, et al., Molecular insight into the formation mechanism of CO2 hydrate in a confined space of surface oxidized porous media system, Fuel 404 (2026) 136254.
[40] M.H. Mahmoodi, M. Manteghian, P. Naeiji, Study the effect of Ag nanoparticles on the kinetics of CO2 hydrate growth by molecular dynamics simulation, J. Mol. Liq. 343 (2021) 117668.

[41] H. Hassanloo, X. Wang, Nanobubbles in graphene-based nanofluids: unraveling the mechanisms behind nucleation, behaviour and thermophysical properties using a molecular approach, Fuel 375 (2024) 132517.
[42] S. Jain, L. Qiao, Molecular dynamics simulations of the surface tension of oxygen-supersaturated water, AIP Adv. 7 (4) (2017).
[43] K. Chae, A. Violi, Mutual diffusion coefficients of heptane isomers in nitrogen: a molecular dynamics study, J. Chem. Phys. 134 (4) (2011).
[44] Q. Yang, C. Zhong, Molecular simulation of adsorption and diffusion of hydrogen in metal– organic frameworks, J. Phys. Chem. B 109 (24) (2005) 11862–11864.
[45] C. Sun, B. Wen, B. Bai, Application of nanoporous graphene membranes in natural gas processing: molecular simulations of CH4/CO2, CH4/H2S and CH4/N2 separation, Chem. Eng. Sci. 138 (2015) 616–621.